Robotica (2009) volume 27, pp. 161–170. © 2008 Cambridge University Press
doi:10.1017/S0263574708004402 Printed in the United Kingdom

Modelling of a special class of spherical parallel manipulators with Euler parameters

Shaoping Bai*†, Michael R. Hansen† and Torben O. Andersen‡

†*Department of Mechanical Engineering, Aalborg University, Denmark*
‡*Department of Energy Technology, Aalborg University, Denmark*

(Received in Final Form: February 4, 2008. First published online: March 27, 2008)

SUMMARY
A method of workspace modelling for spherical parallel manipulators (SPMs) of symmetrical architecture is developed by virtue of Euler parameters in the paper. The adoption of Euler parameters in the expression of spatial rotations of SPMs helps not only to eliminate the possible singularity in the rotation matrix, but also to formulate all equations in polynomials, which are more easily manipulated. Moreover, a homogeneous workspace can be obtained with Euler parameters for the SPMs, which facilitates the evaluation of dexterity. In this work, the problem of workspace modelling and analysis is formulated in terms of Euler parameters. An equation dealing with boundary surfaces is derived and branches of boundary surface are identified. Evaluation of dexterity is explored to quantitatively describe the capability of a manipulator to attain orientations. The singularity identification is also addressed. Examples are included to demonstrate the application of the proposed method.

KEYWORDS: Spherical parallel manipulator; Workspace; Singularity; Dexterity

1. Introduction

Spherical parallel manipulators (SPMs) provide three degrees of freedom of pure rotations which are required for applications such as camera orienting and medical instrument alignment.[1,2,3,4] When dealing with the kinematic design, a key issue is the workspace modelling, which concerns the orientational capability, overall kinematic performance indicated by dexterity as well as the singularities. Up to date, modelling and analysis works on SPMs by adopting different approaches have been reported in technical literature. In the modelling of workspace, Gosselin and Angeles made use of the linear invariants (LI) to explore the workspace of a single leg and then extended the study to the overall manipulator;[5] an orientational representation called "Tilt-and-Torsion angles" was used in the workspace modelling of ref. [6]. A notable numerical approach was adopted in ref. [7], where a solid sphere representing all orientations is partitioned equivolumetrically for a high calculation accuracy. The forward and inverse kinematics were reported in refs. [8, 9, 10], wherein a specific spherical manipulator architecture that leads itself to close-form solutions was considered. The dexterity of a spherical manipulator, which indicates the kinematic accuracy and its controllability, was addressed in refs. [11, 12]. In general, the workspace of an SPM is rather small due to the characteristic of its closed kinematic chain. Design optimizations for a large workspace were reported in refs. [5, 13, 14, 15, 16]. Moreover, SPMs are prone to singularity, which is critical to their controllability. Analyses of singularity can be found in refs. [17, 18]. SPMs with actuator redundancy to eliminate the singularity were presented in refs. [12, 19]. Of the manipulators mentioned, most of them are made of revolute joints, in particular, 3-RRR type manipulators. The research work on other types of SPMs can be found in refs. [20, 21].

Workspace, in the context of this paper, refers to a volume representing all valid rotations of the mobile platform of an SPM. It is regarded as the set of all possible rotations an SPM can attain. The complexity of workspace analysis is related to the presence of multi-loop closed kinematic chains: workspace analysis often yields high-order nonlinear kinematic equations, which are not only functions of the orientation of the end-effector, but also functions of the input angles, i.e., the joint variables. With such kind of equations in which joint variables and link parameters are coupled, it is almost impossible to produce a whole image of the workspace of an SPM. Furthermore, the use of such kinds of equations means that the dexterity evaluation yields only a local performance index, and global measures being further needed.

In this paper, a method of workspace analysis for SPMs is proposed. By decoupling joint variables and architecture parameters, an equation that deals with the global singularity surface is formulated. The equation, independent of joint variables, links the orientational capability of an SPM directly to its architecture parameters. Hence, we term the equation as "equation of mobility", or EOM in short. The EOM is used to identify and visualize the attainable workspace, within which an orientation can be approached by the end-effector from any other orientation. The EOM is also used for the evaluation of dexterity to quantitatively describe overall kinematic performance. Some examples of workspace analysis such as the visualization of boundary surface, singularity identification, and dexterity evaluation by the proposed methods are included.

In exploring SPMs' workspace, we use the Euler parameters to describe the rotation of an SPM, even though most researchers adopt the convention of Euler angles or

* Corresponding author. E-mail: shb@ime.aau.dk

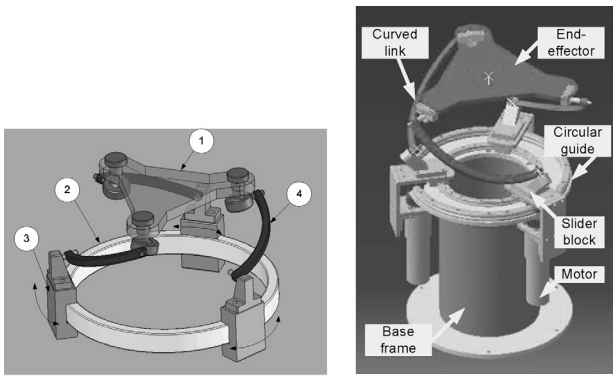

(a) (b)

Fig. 1. An SPM based wrist: (a) Conceptual design with (1) end-effector, (2) circular guide, (3) actuating unit and (4) curved link; (b) an embodiment.

the linear invariants. In the kinematic analysis of spherical manipulators, the importance of rotation representation is often overlooked. As a matter of fact, there exists in manipulators a kind of singularity related to the rotation representation, called *formulation singularity*,[22] which leads to a singular Jacobian for a certain angle of rotation. The singular Jacobian will consequently affect the identification of structural singularities and the evaluation of dexterity. Of the possible representations of rotation, only the Euler parameters, a unit quaternion describing space orientation, is free of singularity.[22,23] For this reason, the Euler parameters are selected in this work to formulate the workspace problem. Moreover, the Euler parameters bring in one additional benefit that a homogenous workspace can be obtained, which has a numeric advantage when volume integration is involved. Furthermore, the use of Euler parameters allows us to formulate rotation equations in polynomial format, which are easier to manipulate than the rotation equations with Euler angles.

The modelling work is carried out for a special class of spherical parallel manipulators, which have a symmetrical architecture with identical legs. The motivation of our research pertains to the design of a novel robotic wrist based on the spherical parallel manipulator,[24] which is to be applied in a humanoid robot being developed at Aalborg University, Denmark. As demonstrated in Fig. 1(a), the SPM consists of three curved links connected to a mobile platform as an end-effector. The three links are driven by three actuators moving independently on a circular guide. This design is kinematically equivalent to an SPM with coaxial input shafts as shown in Fig. 2(b), which was first reported in ref. [13]. Such an architecture enables the end-effector to have an unlimited rolling, in addition to limited pitch and yaw rotations. Compared with Fig. 2(b), the embodiment of Fig. 1(a) improves the design in several aspects. First, the use of circular guide eliminates the three curved links connected to input shafts and keeps only the three links supporting the mobile platform. By introducing the circular guide, the SPM can be designed using a modular approach—all three legs are identical. Moreover, the stiffness of each leg is improved due to the presence of the circular guide. Furthermore, the upper curved links and the mobile platform are connected by spherical joints, rather than revolute ones, which prevent the occurrence of overconstraint of physical revolute joints. From a mechanism viewpoint, this SPM has the same kinematic features as a ball joint and is referred as an *active ball joint*. An embodiment of the active ball joint is shown in Fig. 1(b). In the design, sliders move together with motors via pinion and gear-ring transmissions. Two sets of circular guides from THK Bearings, Japan, are used to enable sliders' high-precision circular motion with small clearance.

2. Modelling of SPM

In general, a spherical parallel manipulator consists of two pyramid-shape platforms, the base platform and the mobile platform connected by three equally spaced legs that each has two links. The axes of all joints, denoted by unit vectors $\mathbf{u}_i$, $\mathbf{v}_i$, and $\mathbf{w}_i$ as shown in Fig. 2(a), intersect at a common center, which is called the center of rotation. The proximal links that are connected to the base platform are assumed to be identical with the common dimension α_1. The distal links that connect to the mobile platform are also assumed to be identical with the common dimension α_2. Moreover, the angles β and γ define the geometry of two regular pyramids

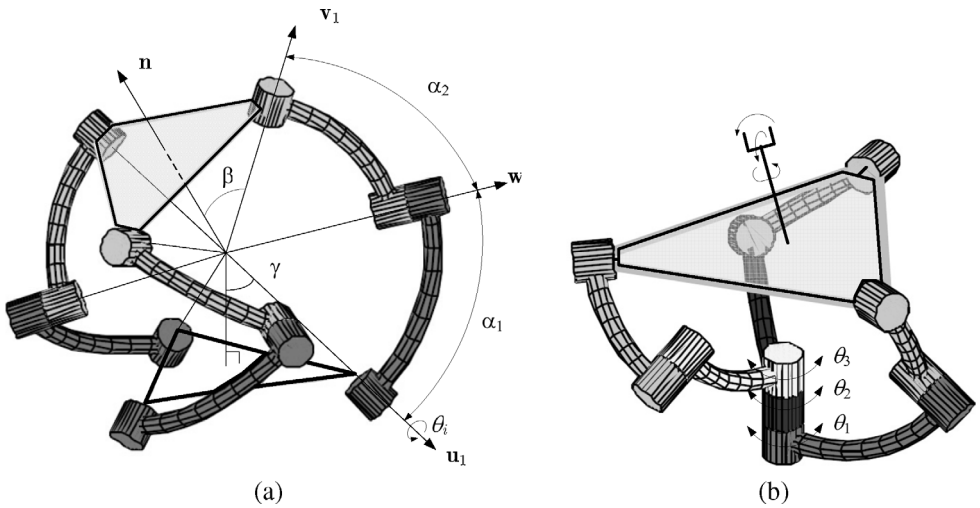

(a) (b)

Fig. 2. Kinematic model of a spherical parallel manipulator: (a) general model; (b) a special case with $\gamma = 0$.

https://doi.org/10.1017/S0263574708004402 Published online by Cambridge University Press

of the base and mobile platforms. The active ball joint is a special case of SPMs for which $\gamma = 0$.

A coordinate system is selected for the SPM, with the origin located at the rotation center. The z axis is normal to the bottom surface of the base pyramid and points upwards, while the y axis is located in the plane made by the z axis and $\mathbf{u}_1$.

By simply applying the geometric rotation, the unit vectors $\mathbf{u}_i$ are derived as:

$$\mathbf{u}_i = [-\sin\eta_i \sin\gamma, \cos\eta_i \sin\gamma, -\cos\gamma]^T \tag{1}$$

where $\eta_i = 2(i-1)\pi/3$.

Unit vectors $\mathbf{w}_i$, $i = 1, 2, 3$ of the axes of the intermediate revolute joints are obtained in terms of the input joint angles θ_i, $i = 1, 2, 3$ as:

$$\mathbf{w}_i = \mathbf{R}_i(\theta_i)\mathbf{z}_y \tag{2}$$

where $\mathbf{z}_y = [0, 1, 0]^T$. The rotation matrix $\mathbf{R}_i(\theta_i)$ can be readily derived from forward kinematics, which is not presented here for clarity. Expanding the right side of Eq. (2) yields

$$\mathbf{w}_i = \begin{bmatrix} -\mathrm{s}\eta_i \mathrm{s}\gamma \mathrm{c}\alpha_1 + (\mathrm{c}\eta_i \mathrm{s}\theta_i - \mathrm{s}\eta_i \mathrm{c}\gamma \mathrm{c}\theta_i)\,\mathrm{s}\alpha_1 \\ \mathrm{c}\eta_i \mathrm{s}\gamma \mathrm{c}\alpha_1 + (\mathrm{s}\eta_i \mathrm{s}\theta_i + \mathrm{c}\eta_i \mathrm{c}\gamma \mathrm{c}\theta_i)\,\mathrm{s}\alpha_1 \\ -\mathrm{c}\gamma \mathrm{c}\alpha_1 + \mathrm{s}\gamma \mathrm{c}\theta_i \mathrm{s}\alpha_1 \end{bmatrix} \tag{3}$$

where s stands for *sine*, and c for *cosine*.

The unit vectors $\mathbf{v}_i$, that are parallel to the axes of the top revolute joints of the legs, are functions of the orientation of the mobile platform. Let this orientation be described by the rotation matrix $\mathbf{Q}$, then

$$\mathbf{v}_i = \mathbf{Q}\mathbf{v}_i^* \tag{4}$$

where $\mathbf{v}_i^*$ are unit vectors of the axes of the top revolute joints when the mobile platform is in its reference orientation, which are given as:

$$\mathbf{v}_i^* = [-\sin\eta_i \sin\beta, \cos\eta_i \sin\beta, \cos\beta]^T \tag{5}$$

The inverse kinematics of SPMs has been well documented in ref. [5]. We briefly review here for completeness.

For the closed chain of the spherical parallel manipulator, the following equations hold:

$$\mathbf{w}_i \cdot \mathbf{v}_i = \cos\alpha_2, \quad i = 1, 2, 3 \tag{6}$$

Substituting Eqs. (3) and (4) into Eq. (6) and further substituting the tan-half identities into the new equation yields

$$A_i t_i^2 + 2B_i t_i + C_i = 0, \quad i = 1,\ 2,\ 3 \tag{7}$$

where $t_i = \tan(\theta_i/2)$. A_i, B_i and C_i are functions of the kinematic parameters and of the orientation of the mobile platform. In these quadratic equations, the three input angles have been decoupled, yielding an inverse kinematic solution to the values of the input angles that correspond to a given orientation.

The forward kinematics, on the other hand, in general, does not yield a close-form solution. To find the orientation corresponding to a set of input angles θ_i, a system of equations needs to be established first. Let $\mathbf{v}_i = [x_i, y_i, z_i]^T$. We have the following equations

$$\mathbf{v}_i \cdot \mathbf{v}_j = \cos\alpha_3, \quad i, j = 1, \ldots, 3, \quad i \neq j \tag{8a}$$

$$\| \mathbf{v}_i \| = 1 \tag{8b}$$

where α_3 is the angle between two lateral edges of the top pyramid. Combining Eqs. (8a) and (8b) together with (6) generates a system of three linear and three quadratic equations, from which possible values of $\mathbf{v}_i$ can be found. The equations can be solved numerically using Newton–Raphson method with selected initial values in order to yield solutions for a certain configuration. The system admits at most eight solutions; a method to find all eight solutions can be found in ref. [10].

The Jacobian matrix of SPMs can be obtained through differentiating Eq. (6), which gives

$$\dot{\mathbf{w}}_i \cdot \mathbf{v}_i + \mathbf{w}_i \cdot \dot{\mathbf{v}}_i = 0 \tag{9a}$$

Note that

$$\dot{\mathbf{v}}_i = \boldsymbol{\omega} \times \mathbf{v}_i \tag{9b}$$

$$\dot{\mathbf{w}}_i = \mathbf{u}_i \times \mathbf{w}_i \dot{\theta}_i \tag{9c}$$

where $\boldsymbol{\omega}$ is the vector of angular velocity of the end-effector. Equations (9a)–(9c) lead to

$$\mathbf{A}\boldsymbol{\omega} = \mathbf{B}\dot{\boldsymbol{\theta}} \tag{10}$$

where $\dot{\boldsymbol{\theta}} = [\dot{\theta}_1, \dot{\theta}_2, \dot{\theta}_3]^T$. Moreover, $\mathbf{A} = [\mathbf{a}_1, \mathbf{a}_2, \mathbf{a}_3]^T$ with $\mathbf{a}_i = \mathbf{w}_i \times \mathbf{v}_i$ and $\mathbf{B} = diag(b_1, b_2, b_3)$

with $b_i = (\mathbf{u}_i \times \mathbf{w}_i) \cdot \mathbf{v}_i$, $i = 1..3$. The Jacobian is finally obtained as $\mathbf{J} = \mathbf{A}^{-1}\mathbf{B}$.

3. Workspace Analysis

Assuming the discriminant of Eq. (7) equal to zero leads to

$$\Delta_i = B_i^2 - A_i C_i = 0, \quad i = 1,\ 2,\ 3 \tag{11}$$

It is pointed out in ref. [5] that Eq. (11) represents a system of equations, each defining a so called *singularity surface*, which separates the leg's mobility region from the immobility region. The global singularity surface, i.e., the singularity surface of the system, can be obtained by intersecting the workspace of the three legs. We show in this work that, when the workspace of a leg is expressed by the surface of the unit sphere in Cartesian space, the mobility region is bounded by two parallel planes, the intersecting lines being the singularity curves.

3.1. Workspace of single leg

We consider first the workspace of a single leg. For simplicity, we analyze the workspace of leg 1, for which $\eta_i = \eta_1 = 0$.

https://doi.org/10.1017/S0263574708004402 Published online by Cambridge University Press

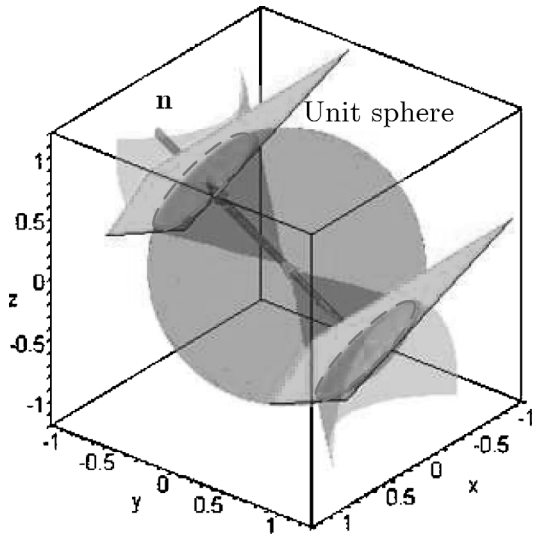

Fig. 3. Workspace of single leg bounded by two planes.

Let $\mathbf{v}_i = [x_i, y_i, z_i]^T$. The coefficient functions A, B and C of Eq. (11) become

$$A_i = y_i(\sin\gamma\cos\alpha_1 - \cos\gamma\sin\alpha_1) - \cos\alpha_2 - z_i(\cos\gamma\cos\alpha_1 + \sin\gamma\sin\alpha_1) \quad (12a)$$

$$B_i = x_i \sin\alpha_1 \quad (12b)$$

$$C_i = y_i(\sin\gamma\cos\alpha_1 + \cos\gamma\sin\alpha_1) - \cos\alpha_2 - z_i(\cos\gamma\cos\alpha_1 - \sin\gamma\sin\alpha_1) \quad (12c)$$

where $i = 1$. By substituting Eq. (12a)–(12c) into Eq. (11) and simplifying, we have

$$\Delta_i = \left[x_i^2 + (y_i\cos\gamma + z_i\sin\gamma)^2\right]\sin^2\alpha_1 - [(y_i\sin\gamma - z_i\cos\gamma)\cos\alpha_1 - \cos\alpha_2]^2 \quad (13)$$

A tedious manipulation on the above equation, not displayed for clarity, finally yields

$$\Delta_i = -(y_i\sin\gamma - z_i\cos\gamma - \cos\alpha_1\cos\alpha_2)^2 + \cos^2\alpha_1\cos^2\alpha_2 + \sin^2\alpha_1 - \cos^2\alpha_2 = 0 \quad (14)$$

which stands for two parallel planes specified by

$$-y_i\sin\gamma + z_i\cos\gamma + D = 0, \ \ i = 1 \quad (15)$$

where

$$D \equiv -\cos\alpha_1\cos\alpha_2 \pm \sqrt{\cos^2\alpha_1\cos^2\alpha_2 + \sin^2\alpha_1\cos^2\alpha_2} = -\cos(\alpha_1 \pm \alpha_2).$$

Equation (15) describes in the simplest possible form of the bounds to the attainable orientations, all being in the region between the two planes. Shown in Fig. 3 is the workspace of a single leg with $\alpha_1 = 60^\circ$, $\alpha_2 = 90^\circ$ and $\gamma = 60^\circ$, displayed with the unit sphere. The two parallel planes specified by Eq. (15) separate the unit sphere into three regions: the region between the two planes is the attainable workspace and the other two are the immobility regions. The two intersections of planes and the sphere are singularity curves, which are the two dashed circles in the figure. The conic surface generated by Eq. (13) is also included in the figure, their intersections with the unit sphere revealing the coincidence of two equations.

Equation (15) of leg 1 can be generalized for the other two legs. The workspace of the other two legs have the same shape as the first leg, but are different in their orientations. Thus the singularity equations of the other two legs can be obtained by rotating an angle η_i around the z-axis, which yields

$$x_i\sin\eta_i\sin\gamma - y_i\cos\eta_i\sin\gamma + z_i\cos\gamma + D = 0, \quad i = 1, 2, 3 \quad (16)$$

or

$$\mathbf{n}_i^T\mathbf{v}_i + D = 0, \quad i = 1, 2, 3 \quad (17)$$

where

$$\mathbf{n}_i = [\sin\eta_i\sin\gamma, -\cos\eta_i\sin\gamma, \cos\gamma]^T.$$

Equation (17) is independent of joint variables and relates the orientation to link dimensions only. In other words, it describes the capability of rotation in terms of the architecture parameters of a leg. For this reason, we named this equation as the equation of mobility, in short, EOM, of a leg.

The distance from the origin to the boundary plane is found as $d = |D|$. Apparently, we have the three cases of the mobility regions of a single leg as listed below:

1. $\alpha_1 \neq \alpha_2$. In this case, d has two distinct values, neither equal to the unit radius. The two planes thus intersect with the unit sphere, yielding three regions. The attainable workspace is the region bounded between two planes, while the immobility regions are outside the two planes. There are two singularity curves that are the intersections of the planes and the sphere.
2. $\alpha_1 = \alpha_2 \neq \pi/2$. In this case, d has two distinct values, one being equal to the unit radius. There is only one plane that intersects the sphere, since the other is tangential to the unit sphere. The spherical surface is divided into two regions by the intersecting plane: one region is the attainable workspace, and the other is the immobility region. Only one singularity curve exists in this case, in addition to a singularity point at the tangential position.
3. $\alpha_1 = \alpha_2 = \pi/2$. In this case, d takes two identical values equal to the unit radius, which implies two planes are tangential to the unit sphere. The attainable workspace consists of the whole sphere, except the two tangential points. There is no singularity curve, but only two singularity points.

From this analysis, three cases of singularity curves corresponding to the three kinds of mobility regions are identified, which is important to the workspace modelling of SPMs. It will be shown later that the singularity surface of the SPM system has three branches, corresponding to the above three cases.

3.2. Equation of mobility with Euler parameters

Vector $\mathbf{v}_i$ of Eq. (17) is a function of the orientation of the end-effector. In describing the spatial orientation, we resort

https://doi.org/10.1017/S0263574708004402 Published online by Cambridge University Press

to Euler parameters in that a rotation matrix expressed by the Euler parameters is free of singularity, in contrast to the Euler angles and the linear invariants, as explained in Introduction. The Euler parameters, expressed as a unit quaternion, are defined as in ref. [23]

$$\mathbf{p} = [e_0, e_1, e_2, e_3]^T = [e_0, \mathbf{e}^T]^T, \quad |e_i| \leq 1, \quad i = 0, \ldots, 3 \tag{18a}$$

with $e_0 = \cos\frac{\phi}{2}; \mathbf{e} = \mathbf{q}\sin\frac{\phi}{2}$ where $\mathbf{q}$ is the unit vector of the axis of a rotation and ϕ is the rotation angle. The unit quaternion implies

$$e_0^2 + \| \mathbf{e} \|^2 = 1 \tag{18b}$$

which stands for that all sets of possible rotations in terms of Euler parameters are located on the surface of a unit hyper-sphere in $\mathbb{R}^4$ given by $[e_0, e_1, e_2, e_3]$. When expressed in $\mathbb{R}^3$ formed by $[e_1, e_2, e_3]$, the hyper-sphere is transformed to a solid sphere which represents all the possible rotations: for each point within the sphere, i.e., $||\mathbf{e}|| \leq 1$, the Euler parameters of rotation is $[\pm r, e_1, e_2, e_3]$, where $r = \sqrt{1 - \mathbf{e}^T\mathbf{e}}$. Hence the solid unit sphere can be used to represent the workspace of an SPM. The sign of r reflects the range of rotations. We take the positive sign which implies $\cos(\phi/2) \geq 0$ or $\phi \in [-\pi, \pi]$.

The rotation matrix in terms of Euler parameters is in a form of

$$\mathbf{Q} = 2\begin{bmatrix} e_0^2 + e_1^2 - \frac{1}{2} & e_1e_2 - e_0e_3 & e_1e_3 + e_0e_2 \\ e_1e_2 + e_0e_3 & e_0^2 + e_2^2 - \frac{1}{2} & e_2e_3 - e_0e_1 \\ e_1e_3 - e_0e_2 & e_2e_3 + e_0e_1 & e_0^2 + e_3^2 - \frac{1}{2} \end{bmatrix} \tag{18c}$$

Substituting Eq. (18c) into Eq. (17) yields polynomial equations of $e_i, i = 0, \ldots, 3$, which are rewritten as:

$$L_ie_0^2 + M_ie_0 + N_i = 0, \quad i = 1, 2, 3 \tag{19}$$

where L_i is independent to $\mathbf{e}$. M_i and N_i are functions of $\mathbf{e}$ of degrees 1 and 2, respectively, as shown in Appendix.

Obviously, it is inconvenient to carry out any analysis with the four orientational variables of Eq. (19). It is thus desired to eliminate one variable from the equations. In doing so, we first substitute Eq. (18b) into Eq. (19) to eliminate the e_0^2 item, which yields

$$M_ie_0 + U_i = 0, \quad i = 1, 2, 3 \tag{20}$$

where

$$U_i = N_i + L_i(1 - ||\mathbf{e}||^2) \tag{21}$$

We rewrite Eq. (20) as

$$M_ie_0 = -U_i, \quad i = 1, 2, 3 \tag{22}$$

Squaring both sides of Eq. (22) and substituting Eq. (18b) into the newly obtained equation yields an equation of $\mathbf{e}$

$$f_i(\mathbf{e}) = M_i^2(1 - ||\mathbf{e}||^2) - U_i^2 = 0 \tag{23}$$

Equation (23) is the EOM of a single leg in terms of the Euler parameters. Since the equation involves the constant D which takes two values, the singularity surface consequently has two branches in general. The two branches may become one, or vanish, depending on the value of D determined by link dimensions, similar to the cases of the singularity curves that are classified in Section 3.1.

Due to the fact that the three legs of an SPM are physically constrained by the top pyramid, the workspace of an SPM is the intersection of the workspace of all three legs. Knowing that the workspace of an SPM is confined by the unit sphere, we can determine the workspace, which is bounded by the sphere surface and the singularity surface, if we can find the singularity surface. With the EOM of Eq. (23), the singularity surfaces of an SPM is obtained by combining that of the individual legs, which is mathematically described by

$$F(\mathbf{e}) = \prod_{i=1}^{3} f_i(\mathbf{e}) = 0 \tag{24}$$

which is a function of $\mathbf{e}$ of degree 12. Corresponding to the singularity surface of a single leg, the singularity surface of an SPM has also two branches in general, which may become one, or vanish, depending on the value of D.

3.3. Singularities

A close-loop kinematic chain like the spherical parallel manipulator has two types of singularities, namely, the Type I and Type II singularities*, according to the classification of Gosselin and Angeles.[25] The singularity surface established with Eq. (24) is exactly the set of singular points of Type I. This can be explained geometrically. The zero discriminant of Eq. (11) means that two solutions to joint variable θ_i are identical. From the point of view of spherical linkages, the two configurations corresponding to the two solutions become one. This leads to a situation of coplanar $\mathbf{u}_i$, $\mathbf{w}_i$ and $\mathbf{v}_i$. In other words, $(\mathbf{u}_i \times \mathbf{w}_i) \cdot \mathbf{v}_i = 0$, $i = 1, 2, 3$, a condition corresponding to $\det(\mathbf{B}) = 0$, i.e., the Type I singularity.[25]

The Type II singularity, on the other hand, occurs when $\det(\mathbf{A}) = 0$. This kind of singularity implies an end-effector moves regardless of the status of the input links and the manipulator is uncontrollable. It is known that Type II singularity is configuration dependent, i.e.,

$$\det(\mathbf{A}) = f(\mathbf{p}; \boldsymbol{\theta}(\mathbf{p})) = 0 \tag{25}$$

To identify the Type II singularity, one must take into account all possible configurations with respect to a certain orientation. But this will end up with a complicated expression for Type II singularity. To avoid the problem with

*There is a third type of singularities in ref. [25], which is actually the combination of the first two types.

https://doi.org/10.1017/S0263574708004402 Published online by Cambridge University Press

the multiple configurations, we treat the identification of Type II singularity as an optimality problem. In doing so, we need only to find Euler parameters and one set of associated joint angles that satisfy Eq. (25) regardless of the configuration. The implementation of this approach is outlined in Section 5 in connection with examples.

4. Evaluation of Dexterity

Dexterity is defined as the capacity of an SPM to provide a large range of orientation to its end-effector. Several measures of dexterity have been proposed, which include the volume of the omnidirectional point-workspace,[26] the volume of attitudinally dexterous point-workspace,[27] and the volume of the controllably dexterous point-workspace,[26] all being defined with respect to serial manipulators. When dealing with spherical parallel manipulators, Gosselin and Angeles used the condition number of the Jacobian matrix as a measure of dexterity.[5] Since the condition number is a function of input angles and cannot reveal the global property of an SPM, Gosselin and Angeles defined further an index called global conditional index (GCI) through the integration of the condition number over the whole workspace.[11]

Now that the EOM of Eq. (24) builds the singularity surface in the Cartesian space, the attainable workspace and dexterity are readily determined.

4.1. Attainable workspace

The volume of an attainable workspace can be calculated through an integral:

$$W = \int_{\Omega} dw \tag{26}$$

where $\mathbf{\Omega}$ denotes a region bounded by the singular surface of Eq. (24) and the surface of the unit sphere. Within the region, the sign of $F(\mathbf{e})$ remains unchanged, a change of sign otherwise implying the reach of the singularity surface. Hence by making use of the equation of motion, W can be precisely calculated by means of definite integral. In practice, taking into account the complexity of the singularity surface, the workspace is evaluated by numerical discretization of the solid unit sphere in order to avoid trivial determination of intervals for the sub-integrals.

The attainable workspace can be normalized with respect to the solid unit sphere. Specifically, the normalized attainable workspace is defined as the ratio of the volume of attainable workspace to the volume of the solid unit sphere, i.e.,

$$\xi = \frac{3}{4\pi} \int_{\Omega} dw \tag{27}$$

The normalized attainable workspace ranges from 0 to 1, a high value implying a large volume of an attainable workspace, and consequently a high mobility.

4.2. Dexterity

The dexterity of a spherical manipulator, following the definition of ref. [11], is

$$GCI = \frac{\int_{\Omega} 1/\kappa(\mathbf{J})\, dw}{\int_{\Omega} dw} = \frac{1}{W} \int_{\Omega} 1/\kappa(\mathbf{J})\, dw \tag{28}$$

with the condition number $\kappa(\mathbf{J})$ is defined as

$$\kappa(\mathbf{J}) = \|\mathbf{J}^{-1}\| \|\mathbf{J}\| \tag{29}$$

where the Euclidean norm $\|\cdot\|$ of a matrix $\mathbf{A}$ is

$$\|\mathbf{A}\| = \sqrt{tr(\mathbf{A}^T \mathbf{W} \mathbf{A})} \tag{30}$$

with $\mathbf{W} = \frac{1}{3}\mathbf{I}$ for the purpose of normalization. Here $\mathbf{I}$ is the 3×3 identity matrix. In practice, the dexterity of Eq. (28) is calculated by a discrete approach

$$GCI = \frac{1}{W} \sum_{w_i \in \Omega} \frac{1}{\kappa_i(\mathbf{J})} dw_i \tag{31}$$

where $\kappa_i(\mathbf{J})$ is the condition number at a discrete point w_i.

Care has to be given to the differential element of the workspace volume dw_i. For a better approximation of the integration, the workspace should be evenly partitioned in all directions, as discussed in refs. [7, 12, 19], which implies the workspace has to be homogeneous. Euler angles do obviously not lead to a homogeneous workspace. To make the element homogeneous, Kurtz and Hayward made use of quaternion coordinates,[19] while Yang and Chen mapped Cartesian workspace into a solid sphere of radius π using exponential coordinates.[7] In this work, a homogeneous workspace is obtained by the introduction of Euler parameters, in a manner similar to that of Kurtz and Hayward, and the workspace is evenly discretized.

5. Examples

We include a few examples of workspace modelling based on the developed method. All simulations were carried out by virtue of Maple 10.

5.1. Visualization of workspace

The equation of motion (EOM) of (24) can be used to visualize the boundary of workspace. Shown in Fig. 4(a) is an example of the singularity surface of an SPM. The dimensions are taken from ref. [1] as $\alpha_1 = 120^\circ, \alpha_2 = 90^\circ$ and $\gamma = \beta = 49.9^\circ$. A cross section $e_3 = 0.6$ of the manipulator's singularity surface is displayed in Fig. 4(b) for a better view, where shadowed areas are immobility regions. In the figure, the outer circle is the section of the unit sphere, which gives the outer boundary. An interconnected region in which the SPM is capable of attending the corresponding orientation can be observed.

As pointed in Section 3.2, there are two branches of singularity surfaces corresponding to the two bounding planes of a single legs. The two branches are displayed in Figs. 4(c) and (d), which are orthogonal.

https://doi.org/10.1017/S0263574708004402 Published online by Cambridge University Press

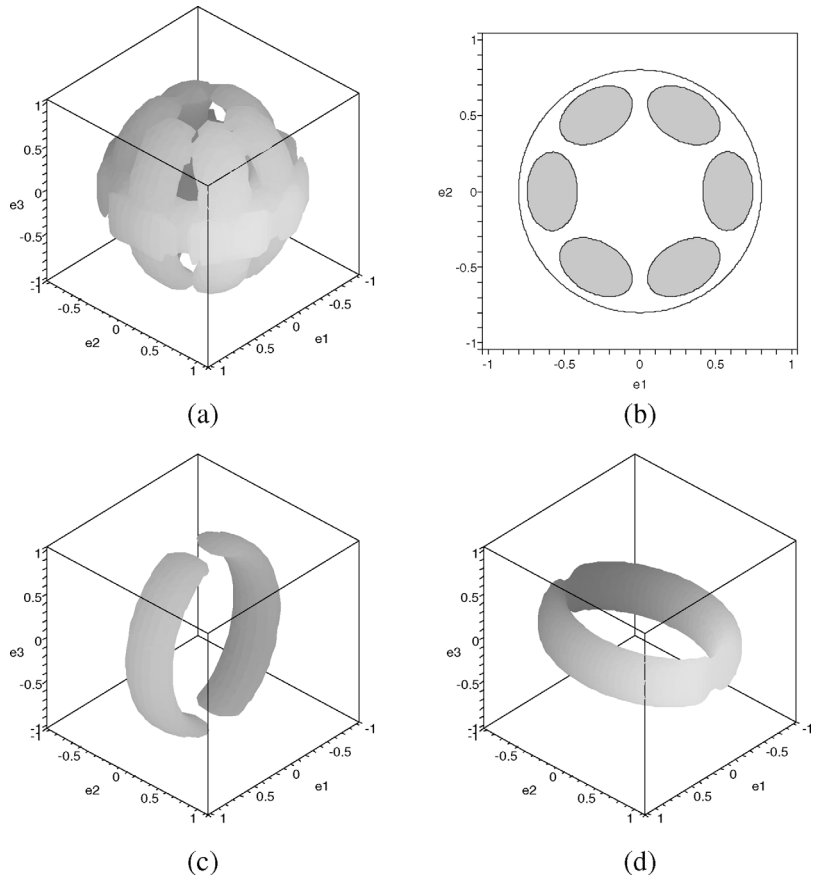

Fig. 4. Singularity surface of an SPM with $\alpha_1 = 120^\circ$, $\alpha_2 = 90^\circ$ and $\gamma = \beta = 49.9^\circ$: (a) the general view; (b) the cross section at $e_3 = 0.6$; (c) & (d) two branches of leg 1.

Shown in Fig. 5(a) is the singularity surface of an SPM with identical dimension of α_1 and α_2. Recall the discussion in Section 3 that the boundary surface with two branches degenerates to a surface with one branch only. This is exactly the case shown in Fig. 5(a). A more clear view of the singularity surface of a single leg is depicted in Fig. 5(b).

5.2. Type II singularities

The Type II singularities are identified numerically for the spherical parallel manipulator with coaxial input shafts. In particular, a solver of nonlinear programs, NLPSolve with Maple 10, is utilized for this purpose. The objective function is defined as $obj = \frac{1}{2}[\det(\mathbf{A})]^2$. The problem of identification of Type II singularities is thus converted to a problem of finding multiple local minima. The constraints applied to the optimization are the three equations shown in Fig. 6. We identify the singularities on layers with different e_3. Each layer is discretized evenly to provide starting points for the solver. The solver will find the nearest local minimum, a singular point. For a coaxial spherical parallel manipulator with dimensions of $\alpha_1 = \alpha_2 = 90^\circ$ and $\beta = 85^\circ$, the distributions of Type II singularity with $e_3 = 0, 0.2, 0.5$ are shown in Fig. 6, where the circle corresponds to the cross section of the unit sphere. It is seen from figure that the

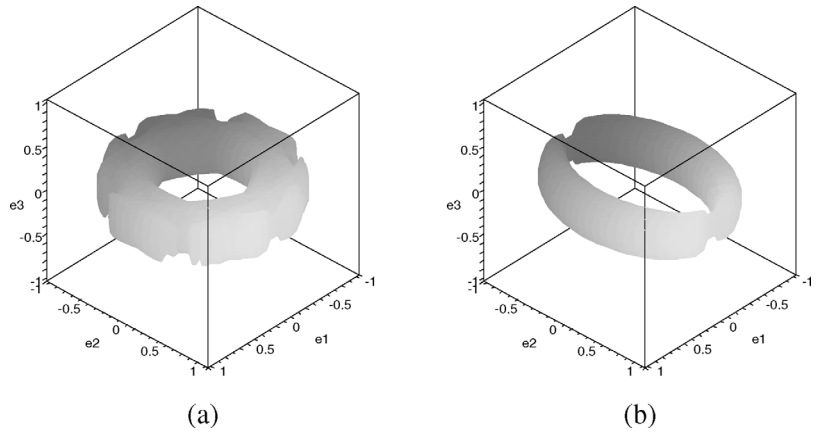

Fig. 5. Singularity surface of an SPM with $\alpha_1 = \alpha_2 = 75^\circ$ and $\gamma = \beta = 49.9^\circ$: (a) the general view; (b) the singularity surface of leg 1.

https://doi.org/10.1017/S0263574708004402 Published online by Cambridge University Press

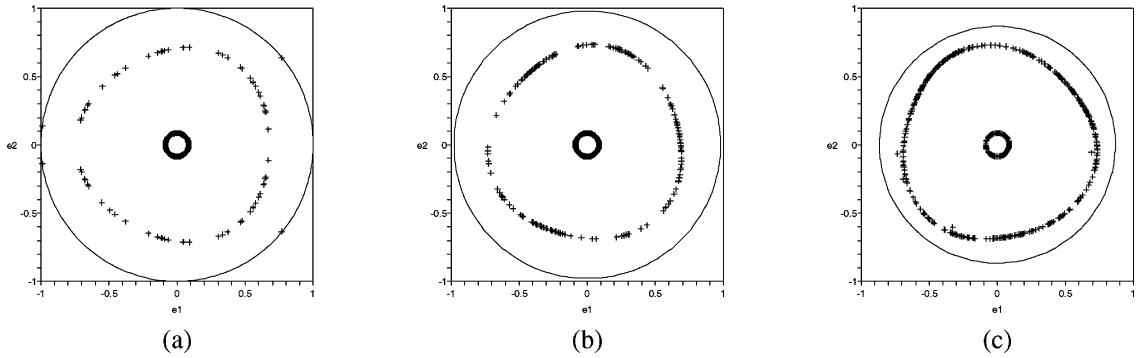

Fig. 6. Type II singularity of an SPM with coaxial input shafts: (a) $e_3 = 0$; (b) $e_3 = 0.2$; (c) $e_3 = 0.5$.

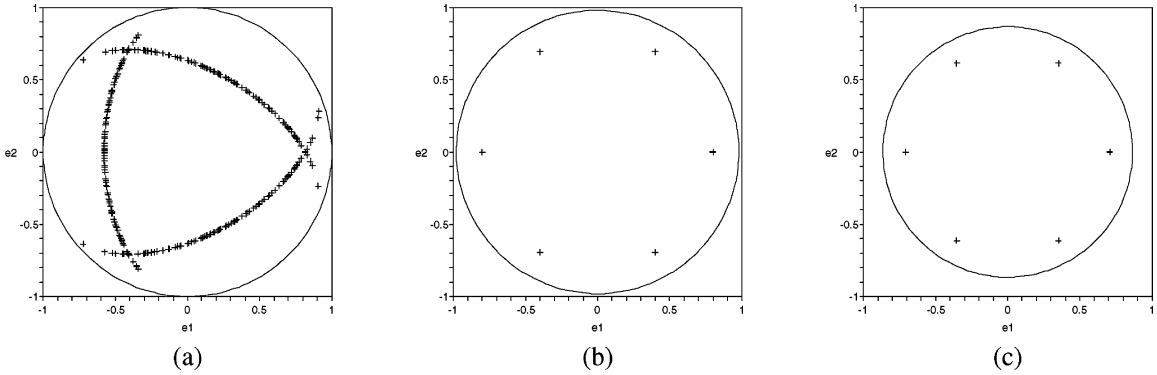

Fig. 7. Type II singularity of the Agile Eye: (a) $e_3 = 0$; (b) $e_3 = 0.2$; (c) $e_3 = 0.5$.

.

method is able to identify both singular points and singular loci. By comparing the distributions over layers, we notice that the layer with $e_3 = 0$ is more prone to singularity than other layers. This is also observed with the case of the Agile Eye. As shown in Fig. 7, the Agile Eye has only six singular points on layers with non-zero e_3.

It is noted that the identified singular points or loci show the possibility of singularity occurred with a certain configuration. Such a configuration, in practice, may not be reached for a manipulator due to mechanical constraints. Shown in Fig. 8 is a configuration of Type II singularity. It shows that some links interference with each other at their joints, which implies the configuration is unlikely reached; the singularity will not occur in this case. In view of this, a real system has to check all possible singularities with respect to mechanical constraints in order to remove those singular points that has no practical effect on the controllability of an SPM.

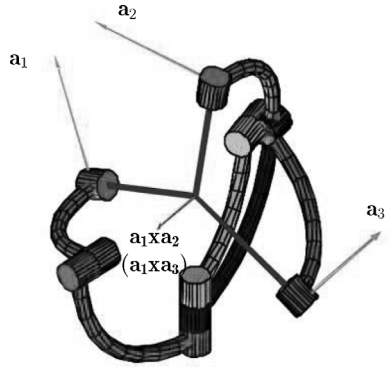

Fig. 8. A configuration of Type II singularity.

5.3. *Evaluation of dexterity*

We demonstrate the evaluation of dexterity with our proposed active ball joint. With $\gamma = 0$ fixed for the active ball joint, the design parameters are α_1, α_2, and β. Given a specified value of β, we can obtain from Eq. (27) the corresponding distributions of attainable workspace ξ against link dimensions α_1 and α_2. We select $\beta = 45^\circ, 60^\circ, 75^\circ$, and 90°, each value yielding a 3D distribution of the dimensionless volume of workspace. Shown in Fig. 9 are distributions of maximum attainable workspace with $\beta = 90^\circ, 75^\circ$, and 60°. In all three cases, the dexterity reaches the maximum with the dimensions of both links being equal to 90°, a coincidence with the results reported in ref. [5].

Using the same procedure as that for the calculation of attainable workspace, the dexterity of SPMs can also be obtained by Eq. (31). Figure 10 shows the distribution of dexterity with $\beta = 90^\circ$. Through comparing Fig. 10 with Fig. 9(a), a noticeable difference between the dexterity distribution and the attainable workspace is observed. The difference suggests that an architecture with maximum workspace cannot guarantee an optimal kinematic performance. While it is desirable to obtain both a high dexterity and a large workspace, a multi-goal optimization is required.[19] Moreover, other factors such as mechanical constraints, static characteristic, etc., have also to be considered. For example, the curved links must avoid collision with each other; a smaller dimension is thus

https://doi.org/10.1017/S0263574708004402 Published online by Cambridge University Press

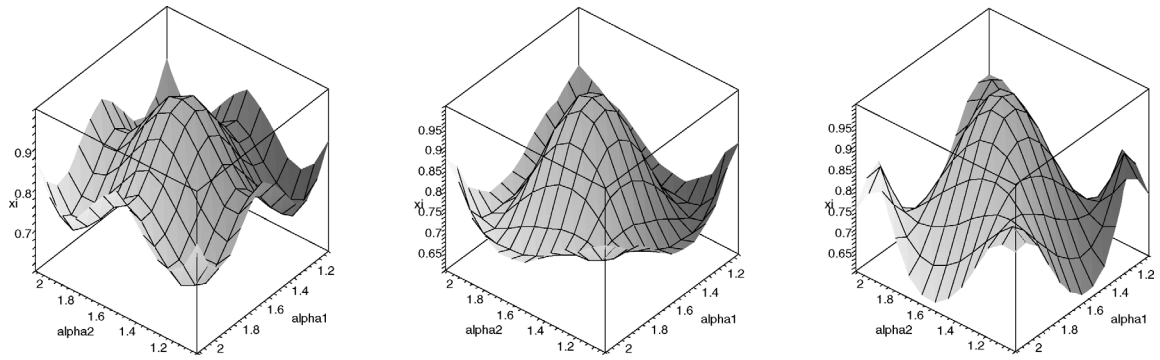

Fig. 9. Attainable workspace distributions with (a) $\beta = 90^\circ$, (b) $\beta = 75^\circ$, and (c) $\beta = 60^\circ$.

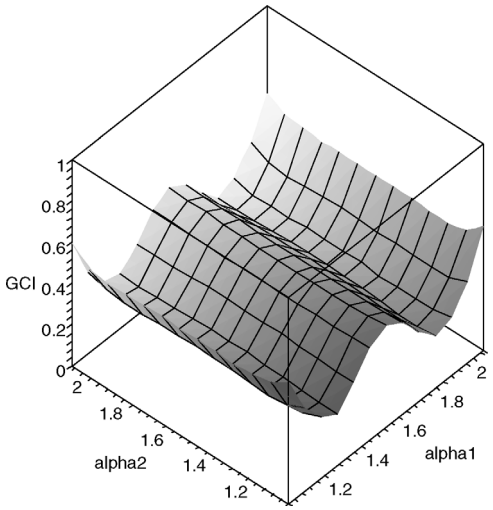

Fig. 10. Dexterity distribution with $\beta = 90^\circ$.

preferred. Furthermore, the static characteristic indicates the capability of load carrying;[13] link dimensions must enable the end-effector to overcome the specified payload. For the case of the active ball joint, the initial dimensions are taken as $\alpha_1 = \alpha_2 = 90^\circ$ and $\beta = 85^\circ$, which are in favor of attainable workspace. The dimensions are under review and subject to change with the above considerations.

6. Conclusions

A novel approach of workspace modelling with Euler parameters is proposed for a special class of spherical parallel manipulators with symmetrical structure. An equation of mobility which describes the boundary surface of an SPM is derived. Based on the workspace model with Euler parameters, dexterity evaluation and singularity identification are explored.

The proposed method, to some extent, can be regarded as an extension of the analysis method reported in ref. [5]. We advance that work by the adoption of Euler parameters with the aim to eliminate the formulation singularity with the rotation representation. We reformulated the problem of workspace modelling in terms of Euler parameters, which provides a solid foundation for the kinematic analysis of SPMs. Furthermore, with Euler parameters, the workspace is established within the solid unit sphere, which is homogeneous for all orientational workspace. Moreover, the branches of singularity surfaces, for both single leg and SPMs, are classified and visualized.

The proposed method offers a unified approach to model and visualize workspace, to identify singularity and to evaluate dexterity. We demonstrate the workspace modelling in connection with the Agile Eye, a well-known spherical manipulator, and the active ball joint. While the method is proposed with respect to a special class of parallel manipulators with symmetrical architecture, it can also be applied to general spherical manipulators and other kinds of parallel manipulators. The extension of the developed modelling method with Euler parameters to other types of parallel manipulators is under consideration.

References

1. C. M. Gosselin and J.-F. Hamel, "The Agile Eye: A High-Performance Three-Degree-of-Freedom Camera-Orienting Device," *IEEE International Conference on Robotics and Automation*, San Diego, CA, USA (1994) pp. 781–786.
2. T. Li and S. Payandeh, "Design of spherical parallel mechanisms for application to laparoscopic surgery," *Robotica*, 20(2), 133–138 (2002).
3. E. Cavallo and R.C. Michelini, "A Robotic Equipment for the Guidance of a Vectored Thrustor," *Proceedings of 35th International Symposium on Robotics (ISR 2004)*, Paris (2004).
4. W. M. Craver and D. Tesar, "Force and Deflection Determination for a Parallel Three Degree of Freedom Robotic Shoulder Module," *ASME 1990 Design Technical Conferences*, Chicago, IL, USA (1990) pp. 473–479.
5. C. M. Gosselin and J. Angeles, "The optimum kinematic design of a spherical three-degree-of-freedom parallel manipulator," *ASME J. Mech. Transm. Autom. Des.* 111, 202–207 (1989).
6. I. A. Bonev and C. M. Gosselin, "Analytical determination of the workspace of symmetrical spherical parallel mechanisms," *IEEE Trans. Robot.* 22(5), 1011–1017 (2006).
7. G.L. Yang and I.-M. Chen, "Equivolumetric partition of solid spheres with applications to orientation workspace analysis of robot manipulators," *IEEE Trans. Robot.* 22(5), 869–879 (2006).
8. R. I. Alizade, N. R. Tagiyiev and J. Duffy, "A forward and reverse displacement analysis of an in-parallel spherical manipulator," *Mech. Mach. Theory*, 29(1), 125–137 (1994).
9. C. M. Gosselin and E. Lavoie, "On the kinematic design of spherical three-degree-of-freedom parallel manipulators," *Int. J. Robot. Res.* 12(4), 394–402 (1993).

https://doi.org/10.1017/S0263574708004402 Published online by Cambridge University Press

10. C. M. Gosselin, J. Sefrioui and M. J. Richard, "On the direct kinematics of spherical three-degree-of-freedom parallel manipulators of general architecture," *ASME J. Mech. Des.* 116(2), 594–598 (1994).
11. C. M. Gosselin and J. Angeles, "A global performance index for the kinematic optimization of robotic manipulators," *ASME J. Mech. Des.* 113(3), 220–226 (1991).
12. S. Leguay-Durand and C. Reboulet, "Optimal design of a redundant spherical parallel manipulator," *Robotica* 15(4), 399–405 (1997).
13. H. Asada and J. Granito, "Kinematic and Static Characterization of Wrist Joints and Their Optimal Design," *IEEE International Conference on Robotics and Automation*, St Louis, MO, USA (1985) pp. 244–250.
14. M. Trabia and J. K. Davidson, "Design conditions for the orientation and attitude of a robot tool carried by a 3-R spherical wrist," *ASME J. Mech. Transm. Autom. Des.* 111, 176–187 (1989).
15. P. M. Larochelle, "Design of 3-dof Spherical Robotic Mechanisms," *Proceedings of the 9th IFToMM World Congress on the Theory of Machines and Mechanisms*, Milan, Itali (1995) pp. 1826–1830.
16. X.-J. Liu, Z.-L. Jin and F. Gao, "Optimum design of 3-dof spherical parallel manipulators with respect to the conditioning and stiffness indices," *Mech. Mach. Theory* 35, 1257–1267 (2000).
17. C. M. Gosselin and J. Wang, "Singularity loci of a special class of spherical three-degree-of-freedom parallel mechanisms with revolute actuators," *Int. J. Robot. Res.* 21(7), 649–659 (2002).
18. I. A. Bonev, D. Chablat and P. Wenger, "Working and Assembly Modes of the Agile Eye," *IEEE International Conference on Robotics and Automation*, Orlando, Florida, USA (2006) pp. 2317–2322.
19. R. Kurtz and V. Hayward, "Multiple-goal kinematic optimization of a parallel spherical mechanism with actuator redundancy," *IEEE Trans. Robot. Autom.* 8(5), 644–651 (1992).
20. X. Kong and C. M. Gosselin, "Type synthesis of three-degree-of-freedom spherical parallel manipulators," *Int. J. Robot. Res.* 23(3), 237–245 (2004).
21. R. Di Gregorio, "Kinematics of a new spherical parallel manipulator with three equal legs: The 3-URC wrist," *J. Robot. Syst.* 18(5), 213–219 (2001).
22. M. Tandirci, J. Angeles and J. Darcovich, "The Role of Rotation Representations in Computational Robot Kinematics," *IEEE International Conference on Robotics and Automation*, Nice, France (1992) pp. 344–349.
23. J. B. Kuipers, *Quaternions and Rotation Sequences: A Primer with Applications to Orbits, Aerospace and Virtual Reality* (Princeton University Press, NJ, 2002).
24. S. Bai and M. R. Hansen, "Evaluation of Workspace of a Spherical Robotic Wrist," *Proceedings of 2007 IEEE/ASME International Conference on Advanced Intelligent Mechatronics*, ETH Zurich, Switzerland (Sep. 4–7, 2007).
25. C. M. Gosselin and J. Angeles, "Singularity analysis of closed-loop kinematic chains," *IEEE Trans. Robot. Autom.* 6(3), 281–290 (1990).
26. J. K. Davidson and K. H. Hunt, "Rigid body location and robot workspace: Some alternative manipulator forms," *ASME J. Mech. Transm. Autom. Des.* 109(2), 224–232 (1987).
27. K. C. Gupta and B. Roth, "Design considerations for manipulator workspace," *ASME J. Mech. Des.* 104(4), 704–711 (1983).

Appendix
Coefficients of Eq. 19

$$L_i = -2\,\mathrm{s}\gamma\mathrm{s}\beta + 2\,\mathrm{c}\gamma\mathrm{c}\beta \tag{32a}$$

$$M_i = 2\,\mathrm{c}\eta_i\mathrm{s}\gamma\mathrm{c}\beta e_1 + 2\,\mathrm{s}\eta_i\mathrm{c}\gamma\mathrm{s}\beta e_2 + 2\,\mathrm{s}\eta_i\mathrm{s}\gamma\mathrm{c}\beta e_2 + 2\,\mathrm{c}\eta_i\mathrm{c}\gamma\mathrm{s}\beta e_1 \tag{32b}$$

$$\begin{aligned} N_i = {} & 4\,\mathrm{s}\eta_i\mathrm{c}\eta_i\mathrm{s}\gamma\mathrm{s}\beta e_1 e_2 - 2\,\mathrm{c}^2\eta_i\mathrm{s}\gamma\mathrm{s}\beta {e_2}^2 - 2\,\mathrm{c}\eta_i\mathrm{s}\gamma\mathrm{c}\beta e_2 e_3 \\ & - 2\,\mathrm{s}\eta_i\mathrm{c}\gamma\mathrm{s}\beta e_1 e_3 + 2\,\mathrm{s}\eta_i\mathrm{s}\gamma\mathrm{c}\beta e_1 e_3 \\ & + 2\,\mathrm{c}\eta_i\mathrm{c}\gamma\mathrm{s}\beta e_2 e_3 - 2\,\mathrm{s}^2\eta_i\mathrm{s}\gamma\mathrm{s}\beta {e_1}^2 \\ & + 2\,\mathrm{c}\gamma\mathrm{c}\beta {e_3}^2 + \mathrm{s}\gamma\mathrm{s}\beta - \mathrm{c}\gamma\mathrm{c}\beta - D \end{aligned} \tag{32c}$$

https://doi.org/10.1017/S0263574708004402 Published online by Cambridge University Press